Magnetic Skyrmion as a Nonlinear Resistive Element: A Potential Building Block for Reservoir Computing

Diana Prychynenko,[1,2,*] Matthias Sitte,[1] Kai Litzius,[1,2,3] Benjamin Krüger,[4] George Bourianoff,[5,†] Mathias Kläui,[1] Jairo Sinova,[1,6] and Karin Everschor-Sitte[1]

[1]*Institute of Physics, Johannes Gutenberg University Mainz, 55099 Mainz, Germany*
[2]*Graduate School of Excellence Material Science in Mainz, 55128 Mainz, Germany*
[3]*Max Planck Institute for Intelligent Systems, 70569 Stuttgart, Germany*
[4]*Institute for Laser Technologies in Medicine and Metrology, University of Ulm, 89081 Ulm, Germany*
[5]*Intel Corporation, 1300 South MoPac Expressway, Austin, Texas 78746, USA*
[6]*Institute of Physics ASCR, v.v.i, Cukrovarnicka 10, 162 00 Praha 6, Czech Republic*

(Received 14 February 2017; revised manuscript received 27 June 2017; published 31 January 2018)

Inspired by the human brain, there is a strong effort to find alternative models of information processing capable of imitating the high energy efficiency of neuromorphic information processing. One possible realization of cognitive computing involves reservoir computing networks. These networks are built out of nonlinear resistive elements which are recursively connected. We propose that a Skyrmion network embedded in magnetic films may provide a suitable physical implementation for reservoir computing applications. The significant key ingredient of such a network is a two-terminal device with nonlinear voltage characteristics originating from magnetoresistive effects, such as the anisotropic magnetoresistance or the recently discovered noncollinear magnetoresistance. The most basic element for a reservoir computing network built from "Skyrmion fabrics" is a single Skyrmion embedded in a ferromagnetic ribbon. In order to pave the way towards reservoir computing systems based on Skyrmion fabrics, we simulate and analyze (i) the current flow through a single magnetic Skyrmion due to the anisotropic magnetoresistive effect and (ii) the combined physics of local pinning and the anisotropic magnetoresistive effect.

DOI: 10.1103/PhysRevApplied.9.014034

I. INTRODUCTION

A. Reservoir computing

Present-day computers are primarily based on advanced CMOS transistors executing Boolean logic functions and, as such, are subject to fundamental trade-offs between energy efficiency and speed. These shortcomings have led to intense worldwide research on alternative modes of computing. There is a strong effort to find energy-efficient models of information processing which are inspired by biological neural networks. These approaches try to imitate neuromorphic information processing models [1]. While CMOS devices appear to be optimal for Boolean logic, implementing alternative models of computation implies using alternative physical systems beyond CMOS. Several approaches to neuromorphic computing are being explored. One example is the concept of reservoir computing (RC) [2–6]. It has long been recognized [7] that some aspects of human cognition can be modeled by recursively connected dynamical systems composed of randomly connected nonlinear devices. However, such systems are difficult to train and hence have been only of very limited practical use. Currently, such systems are realized using fabrics of self-assembled memristive devices [8–17]. The complexity of these networks resembles that of biological brains, in which the complex morphology and interactions between heterogeneous and nonlinear network elements are responsible for powerful and energy-efficient information processing [18]. Unlike designed computation, where each device has a specified role, computation in random resistive element networks does not rely on specific devices in particular roles. Instead, it is encoded in the collective nonlinear dynamic mapping behavior of a network on an applied input signal.

There are two distinct flavors of reservoir computing currently discussed in the literature, referred to as liquid state machines (LSMs) and echo state machines (ESMs) [4]. The two approaches differ in the functionality of the nonlinear elements that lie at the heart of any reservoir computing model. Mathematically, both implementations operate by projecting the applied input signals into a higher dimensional space where sparseness increases and recognition becomes easier. As we show in this paper, magnetic Skyrmion clusters embedded in magnetic substrates can potentially implement either approach to reservoir computing. ESM implementations require a static reservoir of

*Corresponding author.
prychynenko@uni-mainz.de
†Corresponding author.
gibouria@gmail.com

nonlinear elements that projects a spatiotemporal input signal into a high-dimensional output space. The ESM nonlinear elements are characterized by a nonlinear resistance function where the resistance of the element is a function of the time-dependent current profile. A linear neural network can then be efficiently trained to interpret the high-dimensional output representation. The reservoir itself must remain static while that training takes place and during the time that the reservoir is used as a recognition or classification engine. If the internal configuration of an ESM reservoir changes, then the output neural network has to be retrained. Hence, the Skyrmions must remain effectively pinned during this process, which is the motivation to analyze the current interactions with a pinned Skyrmion. Whereas ESMs represent passive neural networks, LSMs use reactive media. The LSM implementation of RC involves network elements that are nonlinear in time and have a spiking behavior [19] and can be created by the movement of Skyrmions within a confined geometry. The LSM implementation of RC is the motivation for studying the Skyrmion trajectory reported here.

Previous research has described reservoirs implemented with memristors, quantum-dot lasers, and atomic switches [20]. Here, we propose using magnetic textures, more precisely Skyrmions, to build an alternative type of RC system which offers potential advantages with respect to size, efficiency, and complexity.

B. Magnetic Skyrmions

Magnetic Skyrmions [21] are chiral spin structures that can be characterized by a topological index, the winding number [22–24]. Because of their topology, they contain quantized amounts of magnetic flux and cannot be unwound easily [24,25], making them robust to defects and impurities [26,27]. They can be created [28–31], read, moved [32–35], and excited [36] via magnetic and electric fields [37–39], spin currents, and magnons [36,40–42].

Skyrmions can be stabilized by various mechanisms, which can be brought down to the interplay of interactions favoring different alignments of the magnetization. As such, they occur in several systems (including metals, semiconductors, and insulators) [43,44] and at different sizes (as small as 1 nm) [28,45]. For example, they also exist in technologically relevant material systems at room temperature [46–49].

Skyrmions occur mostly as either Bloch or Néel type, depending on the details of the antisymmetric exchange interaction. The profile of a Bloch Skyrmion is spiral (spin rotates in the tangential planes), and for a Néel Skyrmion it is cycloidal (spin rotates in the radial planes). There are currently intensive research studies to exploit the full potential of magnetic Skyrmions in spintronics applications, such as ultra-high-density information storage and information processing [50–53]. Proposals to realize "classical computing"—for example, by building Skyrmion-based logic gates [54] and transistors [55]—have been put forward. The use of Skyrmions for probabilistic computing [56], as well as for neuromorphic spiking neural networks [19], has also been proposed.

C. Magnetic Skyrmions for reservoir computing

Recent simulations have shown spontaneous, highly complex, and self-organized patterns of Skyrmions [57] in thin-film configurations which are very well suited for RC. The basic element of such a network is an isolated Skyrmion in a ferromagnetic ribbon. Crucial for RC are the nonlinear current-voltage characteristics of the basic element. For Skyrmions, the nonlinearity has its origin in magnetization-dependent magnetoresistive effects. We stress that the particular type of the magnetoresistance (MR) is not important and that the results of our analysis regarding RC can be transferred as long as the functional relationship between current and voltage for the particular type of MR is nonlinear. Examples of magnetization-dependent magnetoresistive effects are anisotropic magnetoresistance (AMR) and the recently discovered noncollinear magnetoresistive effect [58,59], which has a much larger MR change.

Here, we analyze the contribution of the (noncrystalline) AMR originating from a single Skyrmion that is pinned and embedded in a conducting ribbon. In ferromagnetic samples, the resistance depends on the relative orientation of the magnetization and the direction of the electric current [60]. The AMR effect is caused by anisotropic scattering of the charge carriers in the presence of spin-orbit coupling. The resultant resistivity is commonly larger when the current and the magnetization are parallel, and smaller when they are perpendicular. This difference leads to a distinct contribution of confined spin structures to the resistance, as was previously demonstrated for domain walls [61]. With this work, we pave the way towards Skyrmion-fabrics-based RC.

D. Structure of the paper

In Sec. II, we first describe our approach. We then show in Sec. III our numerical results for the current distribution of single Skyrmions (Bloch and Néel type) embedded in a ferromagnetic background based on the AMR effect. In Sec. III, we also analyze the current-voltage characteristics of an unpinned moving Skyrmion in the conducting channel, illustrating the resistance of the device as a function of the position of the Skyrmion. This sensitivity may be relevant for implementations of liquid state machines or other types of spiking neural networks. In Sec. IV, we consider the nonlinear current-voltage characteristics of a single Skyrmion that is pinned by a local change in the anisotropy. The nonlinear current-voltage relationship of a pinned Skyrmion in a ferromagnetic substrate is required for ESM implementations. In Sec. V, we outline the path to RC with Skyrmion fabrics and substantiate that the results obtained in this work constitute a key step in reaching this goal.

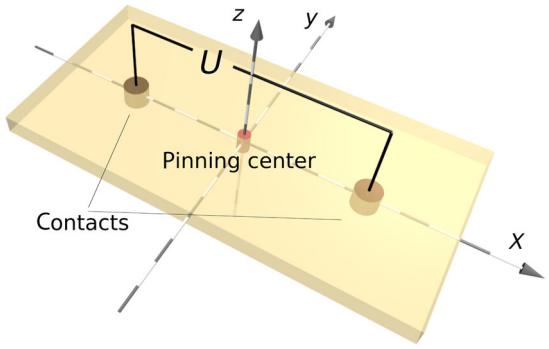

FIG. 1. Schematic plot of the setup. A voltage U is applied between the two contacts of the ferromagnetic thin film. A potential pinning center is located in the center of the film.

II. OUR MODEL

A. Geometry

We consider a metallic ferromagnetic thin film (see Fig. 1) with two metallic contacts embedded on opposite sides of the film, through which we apply a voltage U. In the figure, the coordinate system is chosen such that the magnetic film is placed in the x-y plane. The two contacts are located symmetrically around the center of the ribbon. We prepare an initial state in which a magnetic Skyrmion is stabilized by the Dzyaloshinskii-Moriya interaction (DMI) [62,63] in the center.

B. Physical picture

The significant key ingredient of a RC system are the nonlinear elements building a random, recursive neural network. The nonlinearity in a Skyrmion network is obtained by exploiting spin-torque effects together with magnetoresistive effects. To be more concrete, we consider here a single Skyrmion at the center of the ferromagnetic ribbon. Then we apply a voltage between the two contacts, which leads to a characteristic current flow that we compute based on the AMR effect, as shown in Ref. [64]. The resistance of the "device" is a function of the type, shape, relative size, and position of the Skyrmion in the ribbon. Hence, it is a function of the applied voltage strength.

A pinned Skyrmion is depinned from the impurity above a certain critical current density due to spin-transfer-torque effects [26,27,30,32,34,65]. Below the corresponding voltage, the spin torques causes the Skyrmion to deform. The deformation in the pinned regime, in turn, changes the resistance of the device due to the AMR effect, resulting in its nonlinear current-voltage characteristics. Above a critical voltage, the Skyrmion depins and follows similar trajectories, as is discussed in Sec. III.

C. Numerical model for spin dynamics and current flow

Our numerical simulations are based on the Landau-Lifshitz-Gilbert (LLG) equation for the unit vector field $\boldsymbol{m} = \boldsymbol{M}/M_s$, with the magnetization $\boldsymbol{M}$ and the saturation magnetization M_s. The equation is generalized to include spin-transfer-torque effects [66,67] induced by the electric current, which is calculated self-consistently based on an AMR module [64] due to an applied voltage U between the two contacts. The corresponding LLG equation takes the following form:

$$(\partial_t + \xi \boldsymbol{j}[U,\boldsymbol{m}]\cdot\boldsymbol{\nabla})\boldsymbol{m} = -\gamma \boldsymbol{m}\times\boldsymbol{B}_{\text{eff}} + \alpha \boldsymbol{m}\times\left(\partial_t + \frac{\beta}{\alpha}\xi \boldsymbol{j}[U,\boldsymbol{m}]\cdot\boldsymbol{\nabla}\right)\boldsymbol{m}, \quad (1)$$

where γ is the gyromagnetic ratio, and α and β are the dimensionless Gilbert damping and nonadiabatic spin-transfer-torque parameters, respectively. The prefactor $\xi = P\mu_B/(eM_s)$ is proportional to the current polarization P, with μ_B denoting the Bohr magneton and e the electron charge. The effective magnetic field is given by $\boldsymbol{B}_{\text{eff}} = -M_s^{-1}(\delta F[\boldsymbol{m}]/\delta \boldsymbol{m})$, where F describes the free energy of the system,

$$F = \int \left(A_{\text{ex}}(\boldsymbol{\nabla}\boldsymbol{m})^2 + K_u(1-m_z^2) - \frac{\mu_0}{2}M_S \boldsymbol{m}\cdot\boldsymbol{H}_d[\boldsymbol{m}]\right)dV + F_{\text{DMI}}^{B\,\text{or}\,N}[\boldsymbol{m}], \quad \text{with}$$

$$F_{\text{DMI}}^{B} = \int D_B \boldsymbol{m}\cdot(\boldsymbol{\nabla}\times\boldsymbol{m})dV,$$

$$F_{\text{DMI}}^{N} = \int D_N \boldsymbol{m}\cdot[(\mathbf{z}\times\boldsymbol{\nabla})\times\boldsymbol{m}]dV,$$

where A_{ex} is the exchange constant, K_u is the easy-axis anisotropy strength, and the third term describes the dipolar interactions. F_{DMI}^{B} denotes the Bloch domain wall favoring DMI, while F_{DMI}^{N} refers to DMI favoring Néel walls [62,63,68]. Such interactions, favoring a twisting of the magnetic texture, occur in systems lacking inversion symmetry and originate from spin-orbit coupling. The relaxation of the current happens on a short time scale compared to the dynamics of the magnetization. Therefore, the current $j[U,\boldsymbol{m}]$ can be calculated self-consistently based on the AMR effect [64], where the current density depends on the magnetization through the conductivity tensor $\boldsymbol{\sigma}[\boldsymbol{m}]$ with

$$\boldsymbol{j}[U,\boldsymbol{m}] = -\boldsymbol{\sigma}[\boldsymbol{m}]\cdot\boldsymbol{E}[U]. \quad (2)$$

The electric field $\boldsymbol{E}$ is generated by the applied voltage U, and the corresponding potential is given by $\boldsymbol{E} = -\boldsymbol{\nabla}\Phi$, where Φ satisfies the Poisson equation with the boundary conditions $\Phi|_{c1} = -\Phi|_{c2} = U$ at the two contacts. The conductivity tensor is deduced from the inverse of the resistivity tensor $\boldsymbol{\rho}[\boldsymbol{m}]$. Assuming that the resistivity consists of a material-dependent isotropic part and an anisotropic part that is given by AMR, the resistivity is a function of the angle θ between current and magnetization direction. The local total resistivity is then given by

$$\rho_{\mathrm{tot}} = \rho_{\perp} + (\rho_{\parallel} - \rho_{\perp})\cos^2\theta, \tag{3}$$

where $\rho_{\parallel}$ and $\rho_{\perp}$ denote the resistivities for currents flowing parallel and perpendicular to the magnetization direction. Since the scalar projection of the magnetization in the direction of the current is given by $\cos\theta$, the corresponding tensor takes the form $\boldsymbol{\rho}[\boldsymbol{m}] = \rho_{\perp}\mathbb{1} + (\rho_{\parallel} - \rho_{\perp})\hat{P}[\boldsymbol{m}]$, where the projection operator is given by $\hat{P}[\boldsymbol{m}] = \boldsymbol{m} \otimes \boldsymbol{m}$. Thus, for the conductivity tensor, it follows that

$$\begin{aligned}\boldsymbol{\sigma}[\boldsymbol{m}] &= \frac{1}{\rho_{\perp}}\mathbb{1} + \left(\frac{1}{\rho_{\parallel}} - \frac{1}{\rho_{\perp}}\right)\hat{P}[\boldsymbol{m}] \\ &= \sigma_0\left[\mathbb{1} - \frac{6a}{6+a}\begin{pmatrix} m_x^2 - \frac{1}{3} & m_x m_y & m_x m_z \\ m_y m_x & m_y^2 - \frac{1}{3} & m_y m_z \\ m_z m_x & m_z m_y & m_z^2 - \frac{1}{3}\end{pmatrix}\right], \end{aligned} \tag{4}$$

with $\sigma_0 = (1/\rho_{\parallel} + 2/\rho_{\perp})/3$ and the AMR ratio $a = [(2(\rho_{\parallel} - \rho_{\perp}))/(\rho_{\parallel} + \rho_{\perp})]$, as shown in Ref. [64].

D. Micromagnetic simulations

The method we use is based on micromagnetic simulations which are performed using MicroMagnum [69], including an additional self-written software extension. As previously mentioned, we simulate a quasi-two-dimensional ribbon. For the results shown in Figs. 2–7, the ribbon considered in the simulations is composed of 256×128 cells in the x-y plane and a thickness of one cell in the z direction. The cells correspond to unit cubes of 1 nm edge length. In the center of the ribbon, a cylinder along the z direction is placed with an in-plane radius of 15 nm. Two contacts are modeled as Au cylinders close to the edges of the strip, with a radius of 3 nm; their centers are located at 10% and 90% of the ribbon along the x direction and centered in the y direction. To mimic a pinning center, we position a cylinder of 1.5 nm radius with an enlarged anisotropy strength in the middle of the strip.

The initial magnetic profile corresponds to a ferromagnetic alignment in the z direction, with a saturation magnetization of $M_s = 4.9 \times 10^5$ A m^{-1} but with opposite magnetization of the ribbon and the cylinder. The conductivity of the material is $\sigma_0 = 5 \times 10^6$ S m^{-1}, and its current polarization is $P = 0.56$. Before the dc current is applied, the system needs to be relaxed to the ground state. The single skrymion simulations are performed at a Gilbert damping parameter of $\alpha = 0.25$ and a nonadiabatic spin-transfer-torque parameter of $\beta = 0$.

In contrast to the simulations with a single Skyrmion, the ribbon in the x-y plane used for the data in Fig. 8 is composed of 500×250 cells of 1×1 nm lateral size. Here, to obtain the relaxed magnetization configuration, we start from a completely random state with a saturation magnetization of $M_s = 4.9 \times 10^5$ A m^{-1}. The twisted state is a result of the interplay between the exchange interaction and the DMI. The relaxation process is performed at a large Gilbert damping, $\alpha = 0.5$. The modeling of the contacts is similar to the one used for a single Skyrmion, but with a smaller contact radius of 1 nm. The material has the same conductivity. The spin polarization is $P = 0.5$ and the ratio of the nonadiabatic and adiabatic spin-transfer torque is $(\beta/\alpha) = 0.02$.

The AMR rate which enters the equation for the conductivity tensor and thus affects the magnitude of current density and resistance is set to $a = 1$. The scaling function, f_a, is a function of the magnetization and has been derived from Eq. (4). For in-plane magnetization in the x or y direction, for instance, the scaling function is given by $f_a = -7[(6 + 9a)/(6 + a)]$. Depending on the position, the factor for a ribbon with a Skyrmion may differ from the one without a Skyrmion.

III. CURRENT DISTRIBUTION FOR A SINGLE SKYRMION BASED ON THE AMR EFFECT

In this section, we study the current distribution based on the AMR effect for Bloch and Néel Skyrmions due to the applied voltage.

A. Current profile

The detailed current profiles for Bloch and Néel Skyrmions embedded in a ferromagnetic nanoribbon based on the AMR effect differ. Representative results for the magnetic textures and the corresponding current paths are shown in Figs. 2(a), 2(b), 2(d), and 2(e). To illustrate the bare effect of the Skyrmions, we also substract the current path obtained for the trivial out-of-plane ferromagnetic state; see Figs. 2(c) and 2(f).

The main result is that for the Néel Skyrmion (the upper row of Fig. 2), the current is expelled from the center of the Skyrmion. By contrast, the current density is enhanced in the center for the Bloch Skyrmion. For details of the numerics, see Sec. II D.

The resistance of the device depends not only on the type, shape, and relative size of the Skyrmion with respect to the device but also on its position due to a nonuniform current density. To explore the Skyrmion's position dependence of the resistance, we study the trajectory of the unpinned Skyrmions due to an applied voltage and its resulting current flow.

B. Trajectories of Skyrmions

After applying a voltage (exceeding a threshold value), the Skyrmions move due to spin-transfer-torque effects. Representative Skyrmion trajectories are shown in Fig. 3. Here, the applied voltage is small enough to not noticeably modify the shape of the Skyrmion. Since the total resistance of the device does depend on the position of the Skyrmion, this setup allows for a time-dependent resistance variation at a fixed applied voltage. The relative resistance as a function of time (see Fig. 4) shows how the resistance

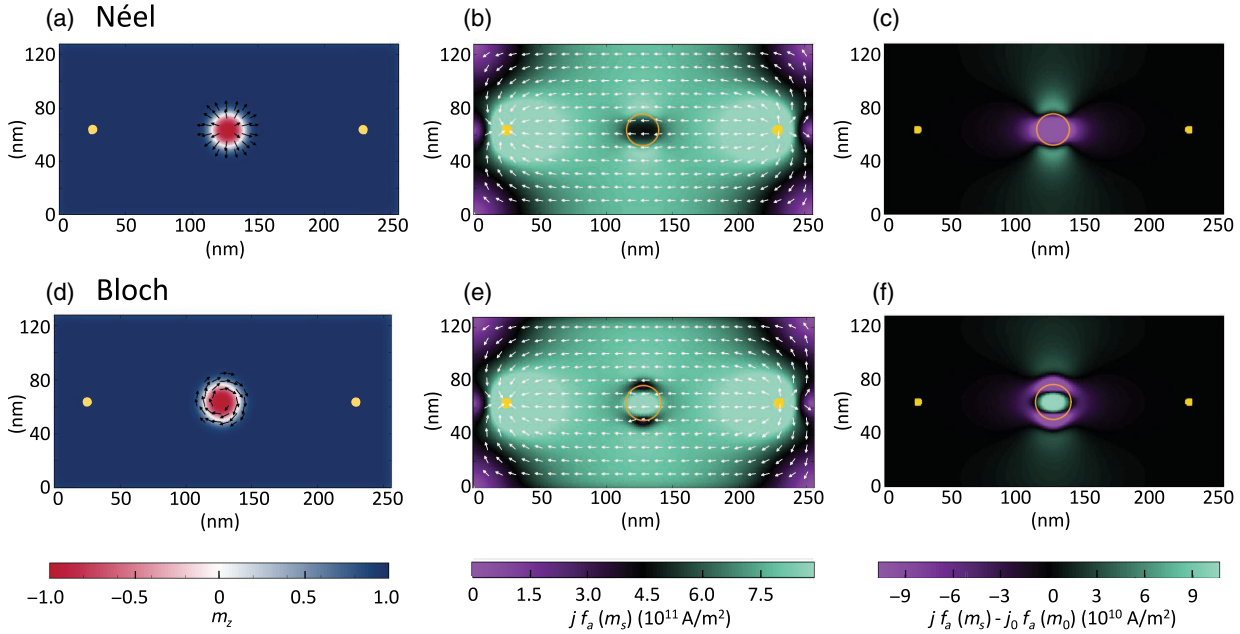

FIG. 2. Magnetization and current profiles for Néel and Bloch Skyrmions shortly after applying a voltage between the contacts (the yellow dots). (a),(d) The magnetization configuration of a Néel and a Bloch Skyrmion, respectively. The color code denotes the out-of-plane component, and the black arrows indicate the in-plane components. (b),(e) The corresponding current flow due to an applied voltage. Here, the color code indicates the current strength and the white arrows refer to the direction of the current. (c),(f) The effect of the Skyrmions after subtracting the current density of the trivial out-of-plane ferromagnetic state. The circle in the current plots indicates the position of the Skyrmion defined by the region where the out-of-plane magnetization vanishes. As can be seen in the plots, the current profiles for the two Skyrmion types differ. For the Néel Skyrmion, the current is expelled from the center and prefers to flow in the x direction tangential to the circle, whereas for the Bloch Skyrmion, the current predominantly flows through the center of the Skyrmion. The parameters used for these simulations are $\alpha = 0.25$, $M_s = 4.9 \times 10^5$ A m^{-1}, $\sigma_0 = 5 \times 10^6$ S m^{-1}, $U = 3.5 \times 10^{-2}$ V, $A_{\mathrm{ex}} = 6 \times 10^{-12}$ J m^{-1}, $K_u = 3 \times 10^5$ J m^{-3}, and $D_{B\,\mathrm{or}\,N} = 1 \times 10^{-3}$ J m^{-2}. These parameters are similar to the ones used in simulations modeling real materials exhibiting Skyrmion physics [46,70]. The value for the bare resistance for this ribbon is given by $R_0 = 348.4\ \Omega$ for the Néel-type and $R_0 = 350.6\ \Omega$ for the Bloch-type Skyrmion. The current densities are scaled with respect to the AMR ratio, a. The scaling function, f_a, increases with a and changes with the local magnetization components. It is constrained by $f_0 = 0$ and $f_1 = 1$. Here, m_s and m_0 refer to the magnetization profiles with and without a Skyrmion, respectively. For further details, see Sec. II D.

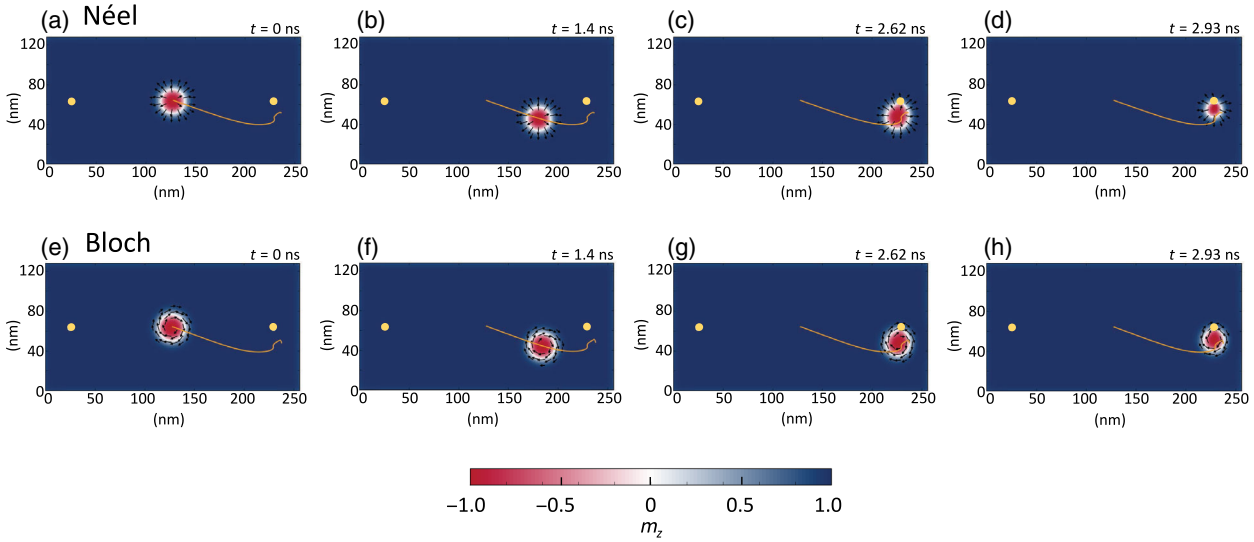

FIG. 3. Evolution in time of Néel (the top row) and Bloch-type (the bottom row) Skyrmions for a fixed voltage. The magnetization profile is encoded in analogy to Figs. 2(a) and 2(d). The parameters used for the simulations are the same as in Fig. 2, meaning that (a) and (e) correspond to Figs. 2(c) and 2(f), respectively. During this motion, a significant deformation of the Skyrmion is observed in the vicinity of the contact only.

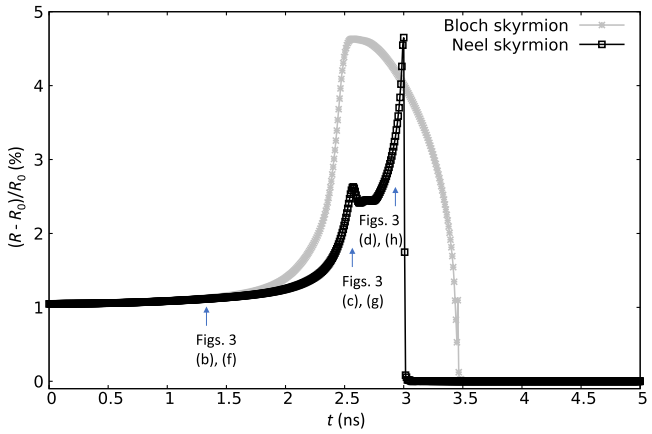

FIG. 4. Relative resistance dependence $(R - R_0)/R_0$ on time for Néel-type and Bloch-type Skyrmions at a fixed voltage. Here, R_0 denotes the resistance of the out-of-plane ferromagnetic configuration in the absence of a Skyrmion. The resistance increases mainly when the Skyrmion approaches the contact until it is absorbed. Details of the curves depend on the magnetization texture; see the discussion in the text. The annotations refer to the magnetization profiles of the Skyrmions at the corresponding times. The parameters used for the simulations are the same as in Figs. 2 and 3. The value for the bare resistance in this geometry is given by $R_0 = 348.4\ \Omega$ for the Néel-type and $R_0 = 350.6\ \Omega$ for the Bloch-type Skyrmion.

changes with time when the Skyrmion is approaching one of the contacts, until it eventually disappears.

The details of the time evolution of the magnetic texture and the corresponding resistances depend on the microscopic parameters of the device. In general, the resistance increases when the Skyrmion approaches the contact since the current density is largest there. The contribution to AMR becomes larger because the resistance is determined by the interplay between the local current density and the magnetization profile; see Eqs. (2)–(4). Depending on the applied voltage strength, a Skyrmion either merges with the contact or passes it. For the parameter set used in Figs. 2, 3 and 4, the Skyrmion disappears at the contact. There, in the vicinity of the contact, the two Skyrmion types display different behavior. The resistance of the Néel-type Skyrmion shows two peaks which can be most intuitively understood when looking at the cross section of the Skyrmion. Its cycloidal domain-wall profile contains two points where the out-of-plane magnetization component is zero, denoted as r_1 and r_2 in the following. The first local maximum in the resistance appears when the first point, r_1, with a large parallel contribution to AMR, touches and eventually merges with the contact. Subsequently, the second point r_2 is moving towards the contact. As it also causes a larger resistance, this merging explains the second maximum. The Bloch-type Skyrmion shows only one peak, namely, when the Skyrmion touches the contact. Since the main contribution to AMR does not come from the connecting line of the contact and the center of the Skyrmion, we do not observe an increase in the resistance when the Skyrmion starts to shrink. When the Skyrmion device is connected in series to a constant current power supply, the nonlinear, time-dependent resistance profile shown in Fig. 4 is represented by a nonlinear time-dependent voltage profile with the same shape. Hence, the depinned Skyrmion device just described can be used to generate voltage spikes required for LSMs.

IV. NONLINEAR *I-V* CHARACTERISTICS FROM LOCAL ANISOTROPY

In this section, we consider the situation where the Skyrmion is pinned at the center of the magnetic ribbon. We model the pinning center by a small cylindrically shaped area in the center of the ribbon with an enhanced out-of-plane anisotropy strength.

The interplay of pinning and spin-transfer torques causes the Skyrmion to deform or stretch, as long as the applied voltage does not exceed a critical depinning threshold. As expected, the deformation is stronger the larger the applied voltage is, as shown in Fig. 5 [30,65]. Since the resistance is a function of the local angle between the current and the local magnetization, it varies with the texture of the Skyrmion and therefore becomes a function of the applied voltage U. Thus, the device has nonlinear current-voltage characteristics with the current-voltage relation

$$\frac{dI}{dU} = G[U, \boldsymbol{m}] = R^{-1}[U, \boldsymbol{m}]. \tag{5}$$

Here, G (R) denotes the differential conductivity (resistance) function depending on the applied voltage U and the magnetic texture $\boldsymbol{m}$. The corresponding behavior of the relative resistance of the device as a function of the applied voltage is plotted in Fig. 6, demonstrating its nonlinear current-voltage characteristics.

Here, all simulations are carried out at zero temperature. Room-temperature operation might affect the results. However, thermal effects are isotropic, and the nonlinear effect shown here arises explicitly from the nonisotropic interplay of the electron current with the magnetic texture. Hence, we expect thermal fluctuations to average out in the system. In Ref. [71], Du *et al.* showed that changes in resistance caused by varying the number of Skyrmions present are still observable at finite temperatures. Furthermore, several works have shown that Skyrmions exist at room temperature [46,49,72,73] and are stable in technologically relevant material systems. In addition, materials can be found for which the Skyrmion phase can be investigated in regions where fluctuations are negligible, i.e., far from the Curie temperature. Moreover, random fluctuations may even have a positive effect on the signals [74,75]—and thus the performance—of RC systems.

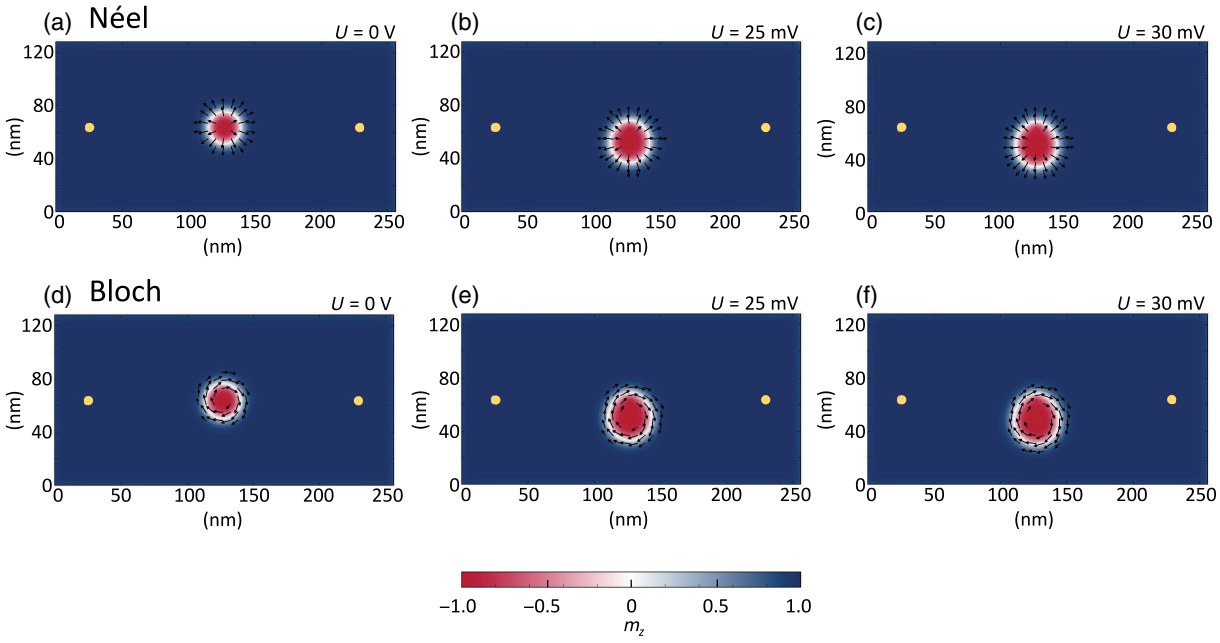

FIG. 5. Deformation of pinned Néel-type, (a)–(c), and Bloch-type, (d)–(f) Skyrmions due to an applied voltage ($U_0 = 0$ V, $U_1 = 2.5 \times 10^{-2}$ V, and $U_2 = 3.0 \times 10^{-2}$ V) which gives rise to a nonuniform current density. With increasing voltage, the deformation increases. The radius r_p and the local anisotropy strength K_p of the pinning center are $r_p = 1.5$ nm and $K_p = 3 \times 10^6$ J m^{-3}, respectively. The remaining parameters have been chosen as follows: $A_{\mathrm{ex}} = 6 \times 10^{-12}$ J m^{-1}, $K_u = 3 \times 10^5$ J m^{-3}, and $D_{B\,\mathrm{or}\,N} = 1 \times 10^{-3}$ J m^{-2}.

In Fig. 7, we vary the DMI and the anisotropy strength and analyze a range in the parameter set for which we obtain Skyrmion configurations that remain pinned when a voltage of $U = 3.0 \times 10^{-2}$ V is applied. The color in this plot encodes the magnitude of the change in resistance. White areas in the phase diagram denote the region where the Skyrmion cannot be stabilized. In general, we conclude that a larger Skyrmion leads to a larger effect. For our finite-size device, the Skyrmion size shrinks when the anisotropy strength is increased, whereas it increases with a larger DMI strength. The latter causes the canting of the local spins to be extended more into the ferromagnetic strip, whereas the domain wall itself is kept narrow.

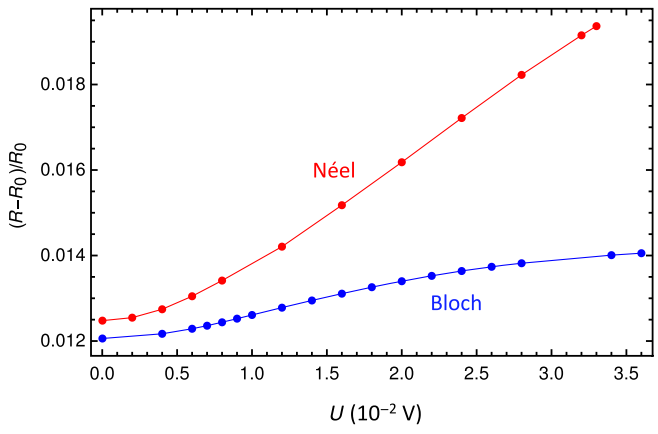

FIG. 6. Relative resistance contribution of a pinned Skyrmion as a function of an applied voltage visualizing the nonlinear behavior of the device. The parameters used are given in Fig. 5.

In the phase diagram, the AMR effect has been studied as a function of the anisotropy and the DMI strength, both of which affect the size of the Skyrmion. However, the resistance also changes with the system width, which emphasizes that the relative size of the Skyrmion with respect to the ribbon plays a crucial role for AMR. The change of the system width is associated with the interplay of two effects which leads first to an increase and later to a reduction of the resistance with a decreasing ribbon width. The resistance increases with a smaller system size since the effect of anisotropy and exchange interaction relative to the DMI is reduced. This scaling result in a larger AMR effect. However, below a critical width, the resistance for a Bloch-type Skyrmion starts to decrease again. With decreasing system width, more current gets pushed from the boundaries towards the center where, for a Bloch-type Skyrmion, the resistance is lowest.

In this section, we analyze the AMR-based behavior of a single Skyrmion confined to a two-dimensional ferromagnetic device. We demonstrate its nonlinear current-voltage characteristics, which make it a promising candidate as a basic element for a reservoir computing network. Changes of the AMR signal within the range we observe in Fig. 6 have been successfully measured [71]. In Ref. [71], Du

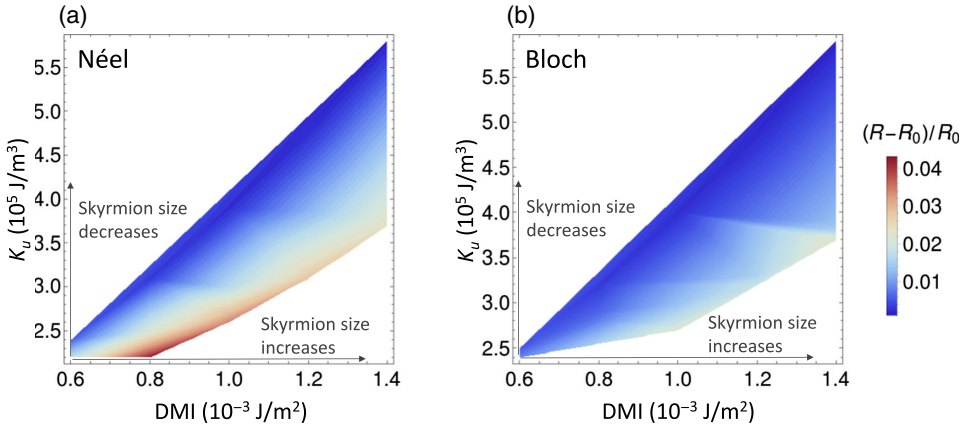

FIG. 7. Relative resistance as a function of the DMI and the anisotropy for (a) a Néel- and (b) a Bloch-type Skyrmion at a fixed voltage, $U = 3.0 \times 10^{-2}$ V. The magnitude of the resistance rises, with increasing Skyrmion size determined by the interplay between the DMI and the anisotropy strength. For the value of exchange coupling and the pinning center, we use the same parameters as in Figs. 5 and 6.

et al. observed quantized jumps in the magnetoresistance when a single Skyrmion was created or annihilated in MnSi nanowires. These jumps can be observed for resistance changes even below 0.1%. Such a resolution is sufficient for the observation of the nonlinear behavior of the relative resistance presented in Fig. 6. Furthermore, Ref. [71] demonstrates the additive nature of the effect for a cluster of Skyrmions, which is important for the configuration we suggest in the next paragraph.

V. THE PATH TO RESERVOIR COMPUTING WITH SKYRMION FABRICS

Thus far, we have discussed the device characteristics of a single Skyrmion in a conducting ferromagnetic wire. To be useful for information processing applications, these single Skyrmions must be connected and arranged into a random, self-assembled, recursively connected configuration. Self-organization can be achieved in a ferromagnetic substrate where, for example, the DMI competes against the exchange interaction, leading to the twisted order configuration shown in Fig. 8(a), exemplified by the Bloch DMI. A current flowing through the magnetic substrate follows the path of least resistance. As imposed by the AMR effect, the current flows between the domain walls, as shown in Fig. 8(b).

Thin films of self-organized Skyrmions connected by current-carrying domain walls bear at least a superficial resemblance to cortical networks of neurons, axons, synapses, and dendrites. Specifically, the above illustration suggests an approach for the implementation of RC systems with Skyrmion-based magnetic substrates. There is a correspondence between the configuration of the magnetic layer shown in Fig. 8(a) and the atomic-switch networks studied in Refs. [11–13]. Here, individual Skyrmions correspond to the silver sulfide (AgS) atomic switches, and the low-resistance parts of the domain walls connecting the Skyrmions correspond to silver (Ag) nanowires. In this analogy, the nonlinear current-voltage relationship of (pinned) Skyrmion devices are used instead of the sinh nonlinear current-voltage relation which characterizes AgS atomic switches. Based on the configurational

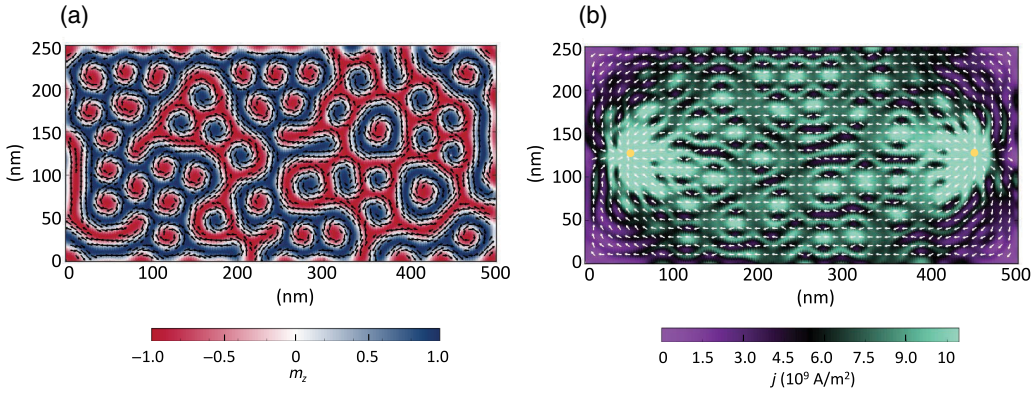

FIG. 8. Magnetization and current profile for magnetic texture including Bloch Skyrmions after applying a voltage between the contacts. (a) The contour plot of the out-of-plane magnetic configuration. The blue and red droplets correspond to Skyrmions. The white lines are domain walls separating the Skyrmions. The arrows indicate the in-plane magnetization. (b) The current path. The parameters used for these simulations are $\alpha = 0.5$, $M_s = 4.9 \times 10^5$ A m^{-1}, $\sigma_0 = 5 \times 10^7$ S m^{-1}, $U = 1.0 \times 10^{-3}$ V, $A_{\mathrm{ex}} = 6 \times 10^{-12}$ J m^{-1}, and $D_B = 2 \times 10^{-3}$ J m^{-2}. For further details, see Sec. II D.

resemblance between Skyrmion networks and atomic-switch networks and the similar nonlinear current-voltage characteristics, we envisage magnetic Skyrmion substrates as a suitable implementation for RC models. Additional analysis will be needed to establish a firm link between this combination of a computational methodology and a physical implementation.

Relative to atomic-switch networks, Skyrmion networks offer several potential advantages for RC implementation. As stated above, Skyrmions have been observed as small as 1 nm, and 10–50 nm diameters are quite common, whereas the elements of atomic-switch networks are a factor of 10–100 larger. Owing to the efficient coupling between conduction electrons and Skyrmions, even low current densities influence the magnetic texture. A rough estimate comparing the power consumption of atomic-switch networks and Skyrmion fabrics shows that Skyrmion systems require about 2 orders of magnitude lower power. Standard voltages used for atomic-switch networks are on the order of 1 V and resistances are about 10 kΩ [10,13,14], leading to a power of $P \approx 100\ \mu$W. For our Skyrmion system, on the other hand, we obtain powers on the order of $P \approx 1\ \mu$W. In general, Skyrmion systems interacting with currents and magnons have many internal degrees of freedom. This complexity results in reservoirs with high tunability and functionality much larger than that for memristors and atomic-switch networks. As shown in Fig. 8, Skyrmions tend to cluster into ensembles of various sizes where each cluster is surrounded by a domain wall. The details of the clustering depend on the competing micromagnetic interaction strengths; therefore, the clustering also should be very sensitive to small bias fields. However, that analysis goes beyond the scope of this work. The present approach is similar to the resistive-switch network but promises to have advantages regarding size, energy efficiency, complexity, and adaptivity, as summarized in the following:

(1) Energy efficiency. The power requirements are potentially low due to an efficient coupling between Skyrmions and currents.
(2) Size. The size of reservoir elements is relatively small. Assuming an average Skyrmion diameter of about 10 nm, a million-element reservoir measures about $10 \times 10\ \mu$m.
(3) Complexity. Skyrmion interactions with currents and magnons yield more internal degrees of freedom than does a simple scalar resistivity associated with memristors and atomic-switch networks.
(4) Adaptivity. High tunability and adjustability of the network topology based on competing micromagnetic forces and applied bias fields.
(5) Homeostatic operation. The system dynamics are sensitive to thermal effects or bias fields applied uniformly to the reservoir. These effects can, in principle, be used to maintain homeostatic operating points.

VI. SUMMARY AND CONCLUSIONS

In this work, we propose Skyrmion systems for reservoir computing and conduct initial analyses. To start with, we show the nonlinear current-voltage characteristics for an isolated Skyrmion pinned in a ferromagnetic strip based on the AMR effect. The particular type of magnetoresitive effect is not crucial to the consequences regarding the application of Skyrmion networks for RC, as other magnetoresistive effects also give rise to the nonlinear properties of such a device. The essential feature is the dependency of the resistance as a function of current density and Skyrmion structure. Our results imply that Skyrmion networks indeed might provide a suitable physical implementation for RC applications.

ACKNOWLEDGMENTS

G. B. appreciates the support of and the useful discussions with Narayan Srinivasa of Intel. We acknowledge funding from the Alexander von Humboldt Foundation, the German Research Foundation DFG (TRR 173 Spin + X), the ERC Synergy Grant SC2 (Grant No. 610115), and the Grant Agency of the Czech Republic (Grant No. 14-37427G). K. E.-S. acknowledges funding from the German Research Foundation (DFG) under Project No. EV 196/2-1. D. P. and K. L. are recipients of a DFG fellowship through the Excellence Initiative by the Graduate School Materials Science in Mainz, Germany (GSC 266), and K. L. thanks the Studienstiftung des Deutschen Volkes for support.

[1] Samuel J. Gershman, Eric J. Horvitz, and Joshua B. Tenenbaum, Computational rationality: A converging paradigm for intelligence in brains, minds, and machines, Science **349**, 273 (2015).
[2] Mantas Lukoševičius and Herbert Jaeger, Reservoir computing approaches to recurrent neural network training, Comput. Sci. Rev. **3**, 127 (2009).
[3] Jens Burger, Alireza Goudarzi, Darko Stefanovic, and Christof Teuscher, Computational capacity and energy consumption of complex resistive switch networks, AIMS Mater. Sci. **2**, 530 (2015).
[4] Mantas Lukoševičius, Ph.D. thesis, Jacobs University Bremen, 2012.
[5] David Verstraeten, Benjamin Schrauwen, Michiel D'Haene, and Dirk Stroobandt, An experimental unification of reservoir computing methods, Neural Netw. **20**, 391 (2007).
[6] Wolfgang Maass, Thomas Natschläger, and Henry Markram, Real-time computing without stable states: A new framework for neural computation based on perturbations, Neural Comput. **14**, 2531 (2002).
[7] Robert Legenstein and Wolfgang Maass, in *New Directions in Statistical Signal Processing: From Systems to Brain*, edited by S. Haykin, J. C. Principe, T. J. Sejnowski, and J. McWhirter, Neural Information Processing Series (MIT Press, Cambridge, MA, 2005), p. 127.

[8] Xiaobin Wang, Yiran Chen, Hai Xi, Hai Li, and Dimitar Dimitrov, Spintronic memristor through spin-thorque-induced magnetization motion, IEEE Electron Device Lett. **30**, 294 (2009).

[9] James P. Crutchfield, William L. Ditto, and Sudeshna Sinha, Introduction to focus issue: Intrinsic and designed computation: Information processing in dynamical systems—Beyond the digital hegemony, Chaos **20**, 037101 (2010).

[10] Audrius V. Avizienis, Henry O. Sillin, Cristina Martin-Olmos, Hsien Hang Shieh, Masakazu Aono, Adam Z. Stieg, and James K. Gimzewski, Neuromorphic atomic switch networks, PLoS One **7**, e42772 (2012).

[11] Tsuyoshi Hasegawa, Takeo Ohno, Kazuya Terabe, Tohru Tsuruoka, Tomonobu Nakayama, James K. Cimzewski, and Masakazu Aono, Learning abilities achieved by a single solid-state atomic switch, Adv. Mater. **22**, 1831 (2010).

[12] Ting Chang, Yuchao Yang, and Wei Lu, Building neuromorphic circuits with memristive devices, IEEE Circuits Syst. Mag. **13**, 56 (2013).

[13] Henry O. Sillin, Renato Aguilera, Hsien-Hang Shieh, Audrius V. Avizienis, Masakazu Aono, Adam Z. Stieg, and James K. Gimzewski, A theoretical and experimental study of neuromorphic atomic switch networks for reservoir computing, Nanotechnology **24**, 384004 (2013).

[14] Adam Z. Stieg, Audrius V. Avizienis, Henry O. Sillin, Cristina Martin-Olmos, Masakazu Aono, and James K. Gimzewski, Emergent criticality in complex turing B-type atomic switch networks, Adv. Mater. **24**, 286 (2012).

[15] Lidan Wang, Xiaodong Wang, Shukai Duan, and Huifang Li, A spintronic memristor bridge synapse circuit and the application in memrisitive cellular automata, Neurocomputing;Variable Star Bulletin **167**, 346 (2015).

[16] Yangqi Huang, Wang Kang, Xichao Zhang, Yan Zhou, and Weisheng Zhao, Magnetic Skyrmion-based synaptic devices, Nanotechnology **28**, 08LT02 (2017).

[17] Steven Lequeux, João Sampaio, Vincent Cros, Kay Yakushiji, Akio Fukushima, Rie Matsumoto, Hitoshi Kubota, Shinji Yuasa, and Julie Grollier, A magnetic synapse: Multilevel spin-torque memristor with perpendicular anisotropy, Sci. Rep. **6**, 31510 (2016).

[18] Olaf Sporns, *Networks of the Brain* (MIT Press, Cambridge, MA, 2016).

[19] Zhezhi He and Deliang Fan, Developing all-Skyrmion spiking neural network, arXiv:1705.02995.

[20] Eleanor C. Demis, Renato Aguilera, Henry O. Sillin, Kelsey Scharnhorst, Eric J. Sandouk, Masakazu Aono, Adam Z. Stieg, and James K. Gimzewski, Atomic switch networks—Nanoarchitectonic design of a complex system for natural computing, Nanotechnology **26**, 204003 (2015).

[21] Sebastian Mühlbauer, Benedikt Binz, F. Jonietz, Christian Pfleiderer, Achim Rosch, Anja Neubauer, Robert Georgii, and Peter Böni, Skyrmion lattice in a chiral magnet, Science **323**, 915 (2009).

[22] Tony H. R. Skyrme, A unified field theory of mesons and baryons, Nucl. Phys. **31**, 556 (1962).

[23] Alexei N. Bogdanov and D. A. Yablonskii, Thermodynamically stable "vortices" in magnetically ordered crystals. The mixed state of magnets, Zh. Eksp. Teor. Fiz. **95**, 178 (1989).

[24] Naoto Nagaosa and Yoshinori Tokura, Topological properties and dynamics of magnetic Skyrmions, Nat. Nanotechnol. **8**, 899 (2013).

[25] Peter Milde, Denny Köhler, Joachim Seidel, L. M. Eng, Andreas Bauer, Alfonso Chacon, Jonas Kindervater, Sebastian Mühlbauer, Christian Pfleiderer, Stefan Buhrandt, Christof Schütte, and Achim Rosch, Unwinding of a Skyrmion lattice by magnetic monopoles, Science **340**, 1076 (2013).

[26] Achim Rosch, Skyrmions: Moving with the current, Nat. Nanotechnol. **8**, 160 (2013).

[27] Jan Müller and Achim Rosch, Capturing of a magnetic Skyrmion with a hole, Phys. Rev. B **91**, 054410 (2015).

[28] Niklas Romming, Christian Hanneken, Matthias Menzel, Jessica E. Bickel, Boris Wolter, Kirsten von Bergmann, André Kubetzka, and Roland Wiesendanger, Writing and deleting single magnetic Skyrmions, Science **341**, 636 (2013).

[29] Wanjun Jiang, Pramey Upadhyaya, Wei Zhang, Guoqiang Yu, Matthias B. Jungfleisch, Frank Y. Fradin, John E. Pearson, Yaroslav Tserkovnyak, Kang L. Wang, Olle Heinonen, Suzanne G. E. te Velthuis, and Axel Hoffmann, Blowing magnetic Skyrmion bubbles, Science **349**, 283 (2015).

[30] Karin Everschor-Sitte, Matthias Sitte, Thierry Valet, Jairo Sinova, and Artem Abanov, Skyrmion production on demand by homogeneous DC currents, New J. Phys. **19**, 092001 (2017).

[31] Ales Hrabec, João Sampaio, Mohamed Belmeguenai, Isabell Gross, Raphael Weil, S. M. Chérif, A. Stashkevich, Vincent Jacques, Andre Thiaville, and Stanislas Rohart, Current-induced Skyrmion generation and dynamics in symmetric bilayers, Nat. Commun. **8**, 15765 (2017).

[32] Tomek Schulz, R. Ritz, Andreas Bauer, Madhumita Halder, Martin Wagner, Chris Franz, Christian Pfleiderer, Karin Everschor, Markus Garst, and Achim Rosch, Emergent electrodynamics of Skyrmions in a chiral magnet, Nat. Phys. **8**, 301 (2012).

[33] Florian Jonietz, Sebastain Mühlbauer, Christian Pfleiderer, Andreas Neubauer, Wolfgang Münzer, Andreas Bauer, T. Adams, Robert Georgii, Peter Böni, Rembert A. Duine, Karin Everschor, Markus Garst, and Achim Rosch, Spin transfer torques in MnSi at ultralow current densities, Science **330**, 1648 (2010).

[34] J. Iwasaki, Masahito Mochizuki, and Naoto Nagaosa, Universal current-velocity relation of Skyrmion motion in chiral magnets, Nat. Commun. **4**, 1463 (2013).

[35] João Sampaio, Vincent Cros, Stanislas Rohart, André Thiaville, and Albert Fert, Nucleation, stability and current-induced motion of isolated magnetic Skyrmions in nanostructures, Nat. Nanotechnol. **8**, 839 (2013).

[36] T. Schwarze, Johannes Waizner, Markus Garst, Andreas Bauer, Ioannis Stasinopoulos, Helmuth Berger, Christian Pfleiderer, and Dirk Grundler, Universal helimagnon and Skyrmion excitations in metallic, semiconducting and insulating chiral magnets, Nat. Mater. **14**, 478 (2015).

[37] Masahito Mochizuki, Spin-Wave Modes and Their Intense Excitation Effects in Skyrmion Crystals, Phys. Rev. Lett. **108**, 017601 (2012).

[38] Johathan S. White, I. Levatić, A. A. Omrani, Nikola Egetenmeyer, Krunoslav Prša, Ivica Živković, Jorge L. Gavilano, Joachim Kohlbrecher, Maciej Bartkowiak,

Helmuth Berger, and Henrik M. Rønnow, Electric-field control of the Skyrmion lattice in Cu_2OSeO_3, J. Phys. Condens. Matter **24**, 432201 (2012).

[39] Naoki Ogawa, Shinichiro Seki, and Yoshinori Tokura, Ultrafast optical excitation of magnetic Skyrmions, Sci. Rep. **5**, 9552 (2015).

[40] Christoph Schütte and Markus Garst, Magnon-Skyrmion scattering in chiral magnets, Phys. Rev. B **90**, 094423 (2014).

[41] Junichi Iwasaki, Aron J. Beekman, and Naoto Nagaosa, Theory of magnon-Skyrmion scattering in chiral magnets, Phys. Rev. B **89**, 064412 (2014).

[42] Olga Petrova and Oleg Tchernyshyov, Spin waves in a Skyrmion crystal, Phys. Rev. B **84**, 214433 (2011).

[43] Xujie Z. Yu, Yoshinori Onose, Naoya Kanazawa, J. H. Park, J. H. Han, Yoshio Matsui, Naoto Nagaosa, and Yoshinori Tokura, Real-space observation of a two-dimensional Skyrmion crystal, Nature (London) **465**, 901 (2010).

[44] Christian Pfleiderer, T. Adams, Andreas Bauer, W. Biberacher, Benedikt Binz, F. Birkelbach, Peter Böni, C. Franz, R. Georgii, M. Janoschek, F. Jonietz, T. Keller, R. Ritz, S. Mühlbauer, W. Münzer, A. Neubauer, B. Pedersen, and Achim Rosch, Skyrmion lattices in metallic and semiconducting B20 transition metal compounds, J. Phys. Condens. Matter **22**, 164207 (2010).

[45] Stefan Heinze, Kirsten von Bergmann, Matthias Menzel, Jens Brede, André Kubetzka, Roland Wiesendanger, Gustav Bihlmayer, and Stefan Blügel, Spontaneous atomic-scale magnetic Skyrmion lattice in two dimensions, Nat. Phys. **7**, 713 (2011).

[46] Seonghoon Woo, Kai Litzius, Benjamin Krüger, Mi-Young Im, Lucas Caretta, Kornel Richter, Maxwell Mann, Andrea Krone, Robert M. Reeve, Markus Weigand, Parnika Agrawal, Ivan Lemesh, Mohamad-Assaad Mawass, Peter Fischer, Mathias Kläui, and Geoffrey S. D. Beach, Observation of room-temperature magnetic Skyrmions and their current-driven dynamics in ultrathin metallic ferromagnets, Nat. Mater. **15**, 501 (2016).

[47] Xujie Z. Yu, Naoya Kanazawa, Yoshinori Onose, K. Kimoto, W. Z. Zhang, Shintaro Ishiwata, Yoshio Matsui, and Yoshinori Tokura, Near room-temperature formation of a Skyrmion crystal in thin-films of the helimagnet FeGe, Nat. Mater. **10**, 106 (2011).

[48] Dustin A. Gilbert, Brian B. Maranville, Andrew L. Balk, Brian J. Kirby, Peter Fischer, Daniel T. Pierce, John Unguris, Julie A. Borchers, and Kai Liu, Realization of ground-state artificial Skyrmion lattices at room temperature, Nat. Commun. **6**, 8462 (2015).

[49] Riccardo Tomasello, Marco Ricci, Pietro Burrascano, Vito Puliafito, Mario Carpentieri, and Giovanni Finocchio, Electrical detection of single magnetic Skyrmion at room temperature, AIP Adv. **7**, 056022 (2017).

[50] Albert Fert, Vincent Cros, and João Sampaio, Skyrmions on the track, Nat. Nanotechnol. **8**, 152 (2013).

[51] Riccardo Tomasello, E. Martinez, Roberto Zivieri, Luis Torres, Mario Carpentieri, and Giovanni Finocchio, A strategy for the design of Skyrmion racetrack memories, Sci. Rep. **4**, 6784 (2014).

[52] Xichao Zhang, G. P. Zhao, Hans Fangohr, J. Ping Liu, W. X. Xia, J. Xia, and F. J. Morvan, Skyrmion-Skyrmion and Skyrmion-edge repulsions in Skyrmion-based racetrack memory, Sci. Rep. **5**, 7643 (2015).

[53] Jan Müller, Magnetic Skyrmions on a two-lane racetrack, New J. Phys. **19**, 025002 (2017).

[54] Jinsong Zhang, Xiao Feng, Yong Xu, Minghua Guo, Zuocheng Zhang, Yunbo Ou, Yang Feng, Kang Li, Haijun Zhang, Lili Wang, Xi Chen, Zhongxue Gan, Shou-Cheng Zhang, Ke He, Xucun Ma, Qi-Kun Xue, and Yayu Wang, Disentangling the magnetoelectric and thermoelectric transport in topological insulator thin films, Phys. Rev. B **91**, 075431 (2015).

[55] Xichao Zhang, Yan Zhou, and Motohiko Ezawa, Antiferromagnetic Skyrmion: Stability, creation and manipulation, Sci. Rep. **6**, 24795 (2016).

[56] Daniele Pinna, Flavio A. Araujo, Joo-Von Kim, Vincent Cros, Damien Querlioz, Perre Bessiere, Jacques Droulez, and Julie Grollier, Skyrmion gas manipulation for probabilistic computing, arXiv:1701.07750v3.

[57] Chun Yeol You and Nam Hui Kim, Critical Dzyaloshinskii-Moriya interaction energy density for the Skyrmion states formation in ultrathin ferromagnetic layer, Curr. Appl. Phys. **15**, 298 (2015).

[58] Christian Hanneken, Fabian Otte, André Kubetzka, Bertrand Dupé, Niklas Romming, Kirsten von Bergmann, Roland Wiesendanger, and Stefan Heinze, Electrical detection of magnetic Skyrmions by tunnelling non-collinear magnetoresistance, Nat. Nanotechnol. **10**, 1039 (2015).

[59] André Kubetzka, Christian Hanneken, Roland Wiesendanger, and Kirsten von Bergmann, Impact of the Skyrmion spin texture on magnetoresistance, Phys. Rev. B **95**, 104433 (2017).

[60] T. McGuire and R. Potter, Anisotropic magnetoresistance in ferromagnetic 3*d* alloys, IEEE Trans. Magn. **11**, 1018 (1975).

[61] Mathias Kläui, C. A. F. Vaz, J. Rothman, J. A. C. Bland, Wolfgang Wernsdorfer, Giancarlo Faini, and Edmond Cambril, Domain Wall Pinning in Narrow Ferromagnetic Ring Structures Probed by Magnetoresistance Measurements, Phys. Rev. Lett. **90**, 097202 (2003).

[62] Igor Dzyaloshinsky, A thermodynamic theory of weak ferromagnetism of antiferromagnetics, J. Phys. Chem. Solids **4**, 241 (1958).

[63] Tôru Moriya, Anisotropic superexchange interaction and weak ferromagnetism, Phys. Rev. **120**, 91 (1960).

[64] Benjamin Krüger, Ph.D. thesis, Universität Hamburg, 2011.

[65] Matthias Sitte, Karin Everschor-Sitte, Thierry Valet, Davi R. Rodrigues, Jairo Sinova, and Ar. Abanov, Current-driven periodic domain wall creation in ferromagnetic nanowires, Phys. Rev. B **94**, 064422 (2016).

[66] Luc Berger, Emission of spin waves by a magnetic multilayer traversed by a current, Phys. Rev. B **54**, 9353 (1996).

[67] John C. Slonczewski, Current-driven excitation of magnetic multilayers, J. Magn. Magn. Mater. **159**, L1 (1996).

[68] André Thiaville, Stanislas Rohart, Émilie Jué, Vincent Cros, and Albert Fert, Dynamics of Dzyaloshinskii domain walls in ultrathin magnetic films, Europhys. Lett. **100**, 57002 (2012).

[69] MicroMagnum—Fast micromagnetic simulator for computations on CPU and GPU, http://micromagnum.informatik.uni-hamburg.de.

[70] Constance Moreau-Luchaire, C. Moutafis, N. Reyren, João Sampaio, C. A. F. Vaz, N. Van Horne, Karim Bouzehouane, K. Garcia, C. Deranlot, P. Warnicke, P. Wohlhüter, J.-M. George, M. Weigand, J. Raabe, V. Cros, and Albert Fert, Additive interfacial chiral interaction in multilayers for stabilization of small individual Skyrmions at room temperature, Nat. Nanotechnol. **11**, 444 (2016).

[71] Haifeng Du, Dong Liang, Chiming Jin, Lingyao Kong, Matthew J. Stolt, Wei Ning, Jiyong Yang, Ying Xing, Jian Wang, Renchao Che, Jiadong Zang, Song Jin, Yuheng Zhang, and Mingliang Tian, Electrical probing of field-driven cascading quantized transitions of Skyrmion cluster states in MnSi nanowires, Nat. Commun. **6**, 7637 (2015).

[72] Xujie Z. Yu, Naoya Kanazawa, W. Z. Zhang, T. Nagai, Toru Hara, Koji Kimoto, Yoshio Matsui, Yoshinori Onose, and Yoshinori Tokura, Skyrmion flow near room temperature in an ultralow current density, Nat. Commun. **3**, 988 (2012).

[73] Olivier Boulle *et al.*, Room-temperature chiral magnetic Skyrmions in ultrathin magnetic nanostructures, Nat. Nanotechnol. **11**, 449 (2016).

[74] Stefano Spezia, Dominique Persano Adorno, Nicola Pizzolato, and Bernardo Spagnolo, Enhancement of electron spin lifetime in GaAs crystals: The benefits of dichotomous noise, Europhys. Lett. **104**, 47011 (2013).

[75] Anderson T. Sergio and Teresa B. Ludermir, in *Proceedings of the 2014 International Joint Conference on Neural Networks (IJCNN), Beijing, 2014* (IEEE, New York, 2014), p. 2653.